Journal of Solid State Chemistry 186 (2012) 23–28

Contents lists available at SciVerse ScienceDirect

Journal of Solid State Chemistry

journal homepage: www.elsevier.com/locate/jssc

An unusual mono-substituted Keggin anion-chain based 3D framework with 24-membered macrocycles as linker units

Haijun Pang, Huiyuan Ma *, Yan Yu, Ming Yang, Ye Xun, Bo Liu **

Key Laboratory of Green Chemical Engineering and Technology College of Heilongjiang Province, College of Chemical and Environmental Engineering, Harbin University of Science and Technology, Harbin 150040, PR China

ARTICLE INFO

Article history:
Received 30 March 2011
Received in revised form
5 November 2011
Accepted 20 November 2011
Available online 1 December 2011

Keywords:
Keggin anion-chain
High dimension
Photocatalysis and electrochemical property

ABSTRACT

A new compound, $[Cu^{I}(H_2O)(Hbpp)_2]\subset\{[Cu^{I}(bpp)]_2[PW_{11}Cu^{II}O_{39}]\}$ (**1**) (bpp=1,3-bis(4-pyridyl)propane), has been hydrothermally synthesized and structurally characterized by single crystal X-ray diffraction. In compound **1**, the unusual –A–B–A–B– array mono-substituted Keggin anion-chains and 24-membered $(Cubpp)_2$ cation-macrocycles are linked together to form a (2, 4) connected 3D framework with channels of ca. 9.784×7.771 Å^2 along two directions, in which the $[Cu(H_2O)(Hbpp)_2]$ coordination fragments as guest components are trapped. The photocatalytic experiments of compound **1** were performed, which show a good catalytic activity of compound **1** for photodegradation of RhB. Furthermore, the IR, TGA and electrochemical properties of compound **1** were investigated.

1. Introduction

Polyoxometalates (POMs) [1–7], as a unique class of inorganic metal oxide clusters, constitute a fascinating class of inorganic systems which is incomparable in structural diversity as well as wide-ranging applications, such as in catalysis [8–14], medicine [15,16], biology [17,18], and materials science [19–26]. Recently, a widespread interest in the POM chemistry is focused on the modification of polyoxoanions by transition-metal complexes (TMCs) to design and synthesis of novel inorganic–organic hybrid compounds that bear both features of inorganic and organic components [27,28]. Especially, the Keggin clusters have been extensively studied to construct the inorganic–organic hybrid compounds by many inorganic chemists due to their classical structure, interesting properties and applications in many fields [29–32]. These efforts have achieved significant results, and many such compounds with high dimensional structures have been successfully synthesized, which can be roughly divided into two types according to integrality of the Keggin clusters in those structures: (i) the compounds are constructed by saturated Keggin clusters and (ii) the compounds are constructed by substituted/vacant Keggin clusters. Because the saturated Keggin clusters usually are more stable than the substituted/vacant ones, the most of the reported compounds based on the Keggin clusters belong to type i [33–40]. In contrast, only several examples of inorganic–organic hybrid compounds are formed by the mono-substituted Keggin anions [41–46], and that constructed by the mono-substituted Keggin anion-chains are even rare [47–49]. Furthermore, only one example of report is about the mono-substituted Keggin anion-chain based compound with a 3D structure [49]. While such compounds can possess the structure feature of Keggin anion-chains and high dimension structures with the unique physical and chemical properties, possibly finding broader applications in the materials science field.

Herein, we report the preparation and structure of a new inorganic–organic hybrid compound based on the mono-substituted Keggin anion-chains, $[Cu^{I}(H_2O)(Hbpp)_2]\subset\{[Cu^{I}(bpp)]_2[PW_{11}Cu^{II}O_{39}]\}$ (**1**) (bpp=1,3-bis(4-pyridyl)propane), which exhibits a 3D framework. The photocatalytic experiments of **1** display a high catalytic activity for photodegradation of RhB with UV irradiation. Furthermore, the electrochemical properties of **1** were also investigated.

2. Experimental section

2.1. Materials and general methods

All reagents were purchased commercially and were used without further purification. Elemental analyses (C, H, and N) were performed on a Perkin-Elmer 2400 CHN Elemental Analyzer. W and Cu were analyzed on a PLASMA-SPEC(I) ICP atomic

* Corresponding author. Fax: +86 45186392716.
** Corresponding author. Fax: +86 45186392701.
E-mail addresses: mahy017@163.com, mahy017@nenu.edu.cn (H. Ma), liubo200400@vip.sina.com (B. Liu).

0022-4596/$ - see front matter © 2011 Elsevier Inc. All rights reserved.
doi:10.1016/j.jssc.2011.11.032

emission spectrometer. The IR spectrum was obtained on an Alpha Centaurt FT/IR spectrometer with KBr pellets in the 400–4000 cm^{-1} region. The thermogravimetric analysis (TGA) was carried out on a Perkin-Elmer TGA7 instrument in flowing N_2 with a heating rate of 10 °C/min. Cyclic voltammogram (CV) was obtained with a CHI 660 electrochemical workstation at room temperature. Platinum gauze was used as a counter electrode, and a Ag/AgCl electrode was referenced. Chemically bulk-modified carbon paste electrode (CPE) was used as a working electrode. Diffuse reflectance UV–vis spectra were obtained with a Varian Cary 500 UV–vis NIR spectrometer.

2.2. Synthesis of $[Cu^{I}(H_2O)(Hbpp)_2] \subset \{[Cu^{I}(bpp)]_2[PW_{11}Cu^{II}O_{39}]\}$ (**1**)

A mixture of $Na_5PW_{11}Cu^{II}O_{39}$ (136 mg, 0.05 mmol), $Cu(CH_3COO)_2 \cdot H_2O$ (160 mg, 0.8 mmol), bpp (40 mg, 0.2 mmol) and 10 mL H_2O was stirred for 1 h. The pH was adjusted to 4.6 with 1 M NaOH, and then the mixture was transferred to an 18 ml Teflon-lined reactor and kept under autogenous pressure at 160 °C for 4 days. After the reactor was slowly cooled to room temperature at a rate of 10 °C/h, dark red crystals of **1** were obtained. The crystals were collected, washed with distilled water, and dried at room temperature (40% yield based on W). Elemental analysis: $C_{52}H_{60}Cu_4N_8O_{40}PW_{11}$ (**1**) (3744.59). Anal. Calcd. for **1**: C, 16.68; H, 1.62; N, 2.99; Cu, 6.79; W, 54.01 (%). Found: C, 16.76; H, 1.69; N, 2.88; Cu, 6.82; W, 53.61 (%). The $Na_5PW_{11}Cu^{II}O_{39}$ was obtained by the following method: The pH of a solution of 1 mol $H_3PW_{12}O_{40} \cdot 12H_2O$ was adjusted to 4.8 using 1 M NaAc. The obtained solution was heated to 90 °C with stirring for 1.5 h. A solution of 1 mol $Cu(NO_3)_2$ in water was added to this hot solution. The solution was heated at 90 °C with stirring for 1 h and filtered cool. The isolated blue solid was designated as $Na_5PW_{11}Cu^{II}O_{39}$, and further characterized by IR spectrum and TGA.

2.3. Preparation of **1**-CPE

The compound **1** modified carbon paste electrode (**1**-CPE) was fabricated as follows: 48 mg of graphite powder and 8 mg of **1** were mixed and ground together by agate mortar and pestle to achieve a uniform mixture, and then 0.6 mL of nujol was added with stirring. The homogenized mixture was packed into a glass tube with a 1.2 mm inner diameter, and the tube surface was wiped with paper. Electrical contact was established with a copper rod through the back of the electrode.

Table 1
Selected crystallographic data for **1**.

Empirical formula	$C_{52}H_{60}Cu_4N_8O_{40}PW_{11}$
M_r	3744.59
Color, habit	Dark red, block
Crystal system	Monoclinic
Space group	*C*2/*c*
a (Å)	25.993(7)
b (Å)	14.628(4)
c (Å)	21.521(5)
β (deg.)	108.245(3)
V (Å^3)	7772(3)
Z	4
D_{calcd} (g cm^{-3})	3.197
F(0 0 0), *e*	6756.0
Refl. measured	10597
Refl. unique	5159
R_{int}	0.0604
[a]R_1/[b]wR_2 [$I > 2\sigma(I)$]	0.0586/0.1679
GoF (F^2)	0.869

[a] $R_1 = \sum||F_o| - |F_c|| / \sum|F_o|$.
[b] $wR_2 = \sum[w(F_o^2 - F_c^2)^2] / \sum[w(F_o^2)^2]^{1/2}$.

2.4. Single crystal X-ray

Crystal data for compound **1** were collected on a *Bruker SMART-CCD* diffractometer, with Mo*K*α monochromatic radiation (*λ* = 0.71073 Å) at 293 K. The structure of **1** was solved by direct methods and refined by full-matrix least-squares on F^2 using the *SHELXTL* crystallographic software package [50,51]. The organic hydrogen atoms were generated geometrically. The hydrogen atoms of water molecule in compound **1** could not be introduced in the refinement but were included in the structure factor calculation. The crystal data and structure refinement of **1** is summarized in Table 1.

3. Results and discussion

Compound **1** was synthesized under hydrothermal conditions. All W atoms are in the +VI oxidation state confirmed by bond valence sum (BVS) calculations [52]. The Cu1 and Cu2 in **1** are all in the +I oxidation state, confirmed by their "T"-type coordination environments and BVS calculations. The partial reduction of Cu^{II} into Cu^{I} is often observed in the hydrothermal reaction systems, which may be attributed to the excess of the N-containing ligand [34,53,54]. The Cu3 is in the +II oxidation state, confirmed by its octahedral coordination environment and BVS calculation. Since **1** was isolated from acidic aqueous solution, two protons were attached to the uncoordinated N atoms of the two bpp molecules to compensate charge balance, which is similar to the case of $\{[Ag(bipy)]_4[P_2W_{18}O_{62}]\} \cdot 2[Hbipy]$ and $K[P_2W_{18}O_{62}] \cdot 2.5[H_2bipy] \cdot 2H_2O$ [55], then **1** is formulated as $[Cu^{I}(H_2O)(Hbpp)_2] \subset \{[Cu^{I}(bpp)]_2[PW_{11}Cu^{II}O_{39}]\}$.

3.1. Crystal structure

Single-crystal X-ray diffraction analysis reveals that **1** consists of three crystallographically distinct motifs: a coordination fragment $[Cu^{I}(H_2O)(Hbpp)_2]^{3+}$ (**I**), a 24-membered macrocycle $[Cu^{I}(bpp)]_2^{2+}$ (**II**) and one mono-substituted Keggin anion-chain $[PW_{11}Cu^{II}O_{39}]_n^{5n-}$ (**III**) (Fig. 1). In motif **I** (Fig. 1 **I**), Cu2 atom is tri-coordinated in a "T"-type coordination geometry achieved by two nitrogen atoms of two "Z"-typed conformation bpp molecules and one H_2O molecule. The bond distances around the Cu2 atom are 1.89–1.96 Å (Cu–N) and 1.89–2.73 Å (Cu–O), and the N–Cu–N angles are 166.60–170.67°. By these coordination modes, the Cu^{I} atom links two bpp molecules and one H_2O molecule forming a coordination fragment $[Cu^{I}(H_2O)(Hbpp)_2]^{3+}$. The Cu1 atoms in motif **II** (Fig. 1 **II**) are also in a "T"-type coordination environment achieved by two nitrogen atoms of two bpp molecules and one oxygen atom from the Keggin anion-chain $[PW_{11}Cu^{II}O_{39}]_n^{5n-}$, but differently they are bridged by two "U"-typed conformation bpp ligands to form a 24-membered macrocycle $[Cu^{I}(bpp)]_2^{2+}$ with the edges of 10.550 and 9.699 Å, and twisting angles of 120.18°, indicating a distorted square geometry. The bond distances around the Cu1 atom are 1.865 Å (Cu–N) and 2.94 Å (Cu–O), and the N–Cu–N angle is 178.7°. Note that the distance of Cu1–O18 (2.94 Å) is shorter than the sum of the van der Waal's radii of Cu and O (3.19 A°) [56], implying along-range coordinative bond, which is similar to the compounds reported [57]. The motif **III** (see Fig. 1 **III**) consists of the mono-substituted Keggin cluster $[PW_{11}Cu^{II}O_{39}]^{5-}$, in which the substituted atom Cu3 is statistically distributed on two opposite sites with a tungsten atom W6 (the occupancy of the Cu3 and W6 atoms were 50% after refining). There exist two kinds of arrays (A and B) for the Keggin clusters in

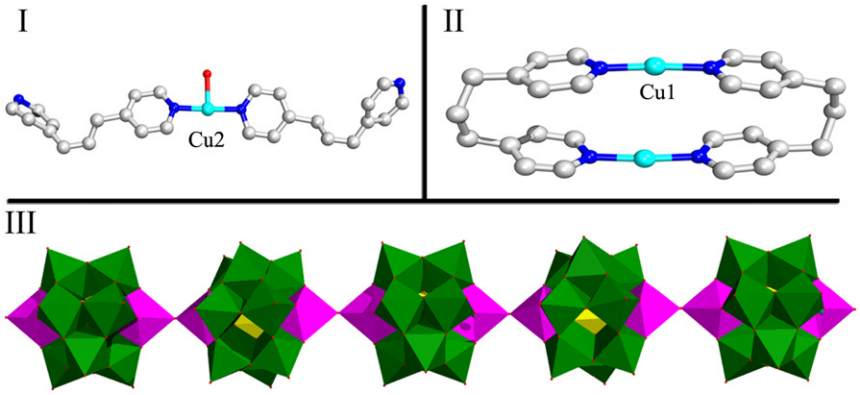

Fig. 1. Three crystallographically distinct motifs in **1**: **I**, $[Cu^{I}(H_2O)(Hbpp)_2]^{3+}$ coordination fragment; **II**, $[Cu^{I}(bpp)]_2^{2+}$ 24-membered macrocycle; **III**, $[PW_{11}Cu^{II}O_{39}]_n^{5n-}$ mono-substituted Keggin anion-chain.

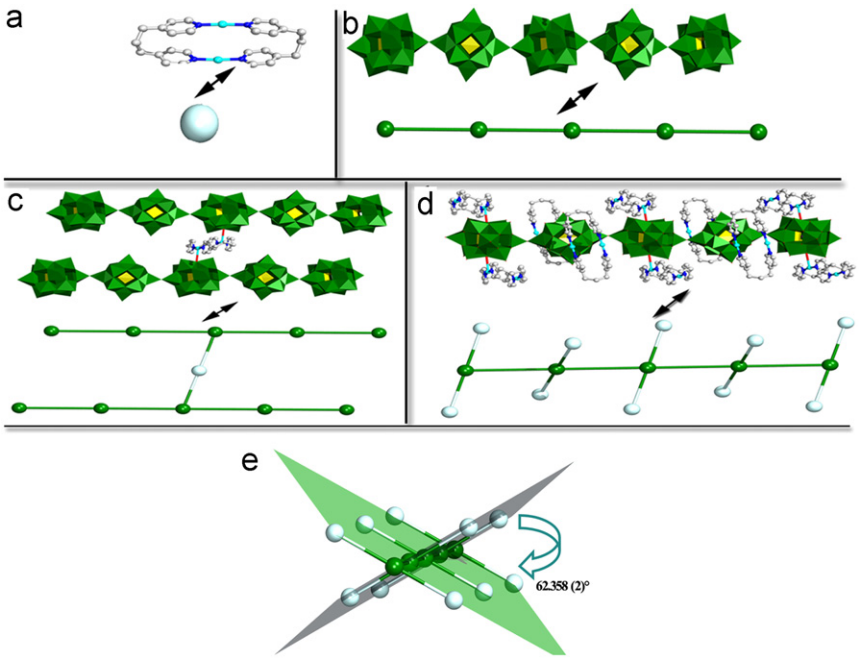

Fig. 2. Schematic figures: (a) $[Cu^{I}(bpp)]_2^{2+}$ 24-membered macrocycle; (b) $[PW_{11}Cu^{II}O_{39}]_n^{5n-}$ mono-substituted Keggin anion-chain; (c) the connect model between neighboring Keggin anion-chains; (d) the connect model between the anion-chain and the macrocycle; and (e) the angle of two planes formed by one anion-chain and its coordinated macrocycles.

motif **III**: A cluster that rotates clockwise for ~180° can obtain B cluster (Fig. S1 top). Furthermore, the neighboring A and B clusters are alternately connected via sharing the O2 atoms to form a straight chain $[PW_{11}Cu^{II}O_{39}]_n^{5n-}$ in –A–B–A–B– array (Fig. S1 middle and bottom), which is different from the usual –A–A–A–A– array ones [47–49] (Fig. S2).

One structural feature of **1** is that mono-substituted Keggin anion-chains (motif **III**) form a 3D framework with a 24-membered macrocycles (motif **II**) as linkers. On the one hand, each of the 24-membered macrocycles connects two adjacent anion-chains by sharing the O18 atoms with two $[PW_{11}Cu^{II}O_{39}]^{5-}$ anions of the two anion-chains (Fig. 2a–c). On the other hand, each of the anion-chains was connected by four 24-membered macrocycles from different directions (Fig. 2a, b, d, and e). Consequently, a new 3D structure is formed by repeating these interesting connections (Fig. S3). The topological analysis of the structure has been performed by considering each $[Cu^{I}(bpp)]_2^{2+}$ macrocycle as a 2-connected node (Fig. 2c) and each $[PW_{11}Cu^{II}O_{39}]^{5-}$ cluster as a 4-connected node (Fig. 2d), which can be symbolized as a network with a $(8^4 \cdot 12^2)$ topology, shown in Fig. 3.

Another fascinating structural feature of **1** is its highly opened 3D framework. The 3D framework of **1** contains channels with dimensions of ca. 9.784×7.771 Å^2 along the two different directions as shown in Figs. 4 and 5, in which the $[Cu^{I}(H_2O)(Hbpp)_2]^{3+}$ coordination fragments as guest components are trapped. Calculations by PLATON reveal that the van der Waals free space per unit cell (after the guest $[Cu^{I}(H_2O)(Hbpp)_2]^{3+}$ coordination fragments have been removed) is approximately 3087.4 Å^3, corresponding to 39.7% of the crystal volume 7772.0 Å^3.

3.2. IR spectrum, TGA and PXRD patterns

In the IR spectrum (see Fig. S4), the peaks at 952.67, 887.1 and 809.9 cm^{-1} are attributed to $\nu(W{=}O_t)$, $\nu_{as}(W{-}O_b{-}W)$ and $\nu_{as}(W{-}O_c{-}W)$ vibrations of α-Keggin cluster (O_t = terminal oxygen, O_b = bridged oxygen of two octahedral sharing a corner, O_c = bridged oxygen of two octahedral sharing an edge), respectively. The

informative bands at 1097.7 and 1062.6 cm^{-1} can be assigned to the P–O stretching vibrations in **1**. Compared with a typical value of about 1067 cm^{-1} for the Keggin anion [58,59], the P–O stretch of the mono-substituted Keggin tungstophosphate ion splits into two bands because of the lower symmetry than that in the T_d parent Keggin [49]. The bands at 1424.9–1618.01 cm^{-1} region are assigned to characteristic peaks of the bpp ligands. Additionally, the band at 3442.3 cm^{-1} is ascribed to characteristic peak for water molecules.

The TGA of **1** was performed in air at a rate of 10 °C/min in the range of 45–600 °C to explore its thermal stability. The TGA curve of **1** exhibits two weight loss steps (Fig. S5). The first weight loss is 11.61% below 318 °C and the second weight loss is 10.22% occurred in the range of 318–400 °C. The weight loss step for the coordinated water molecules (calc. 0.48%) is not obviously observed, which is possible because the amount of the water molecules is little. Given a detailed analysis and comparison between the thermal behavior of **1** and its structure, it can be deduced that the thermal decomposition of bpp molecules in two steps may be attributed to their different coordinated modes, namely, the thermal decomposition 11.61% (calc. 11.08%) before 380 °C corresponds to the loss of water molecules and half of the amount of bpp molecules in the $[Cu^{I}(H_2O)(Hbpp)_2]^{3+}$ fragment and then another half of the amount of bpp molecules in the $[Cu^{I}(bpp)]_2^{2+}$ macrocycle 10.22% (calc. 10.60%) suffered a rapid transformation process in higher temperature. The total weight loss is 21.83%, in consistence with the calculated value of 22.14% and also supporting the chemical composition of **1**.

The *PXRD* patterns for **1** are presented in Fig. S6. The diffraction peaks of both simulated and experimental patterns match well, indicating the phase purities of **1**.

3.3. Electrochemical property

Compound **1** is insoluble in water and common organic solvents. Thus, the bulk-modified carbon paste electrode (CPE) becomes the optimal choice to study the electrochemical properties. The electrochemical behavior of a **1**-modified carbon paste electrode (**1**-CPE) was investigated in 1 M H_2SO_4 aqueous solution at different scan rates (Fig. 6 left). In the potential range of +600 to −600 mV, there exist three reversible redox peaks II–II′, III–III′ and IV–IV′, attributed to the redox process of $W^{VI/V}$ in the PW_{12} polyanions [60]. This result shows that **1** is a moderate ground-state oxidant with widely differing reduction potentials, and exhibits an ability to undergo a series of reversible redox cycles without chemical decomposition. This feature has significant implications for **1** as a photocatalyst in an essential photocatalytic system with respect to reduction of catalyst and regeneration of reduced catalyst [61]. In addition, the irreversible anodic peak I is assigned to the oxidation of the Cu(I) centers [62]. The peak currents of IV are linearly proportional to the scan rates (see Fig. 6 right), indicating a possible surface-controlled redox process [63].

3.4. Photocatalysis property

Rhodamine-B (RhB) as an example of dye contaminant can be used for evaluating activity of a photocatalyst in purification of

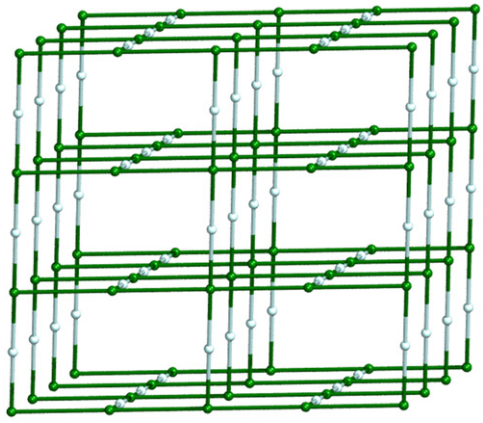

Fig. 3. Schematic view of the $(8^4 \cdot 12^2)$ topology in **1**. Color codes: green, four-connected node of one $[PW_{11}Cu^{II}O_{39}]^{5-}$ cluster; blue, two-connected node of $[Cu^{I}(bpp)]_2^{2+}$ macrocycle. (For interpretation of the references to color in this figure legend, the reader is referred to the web version of this article.)

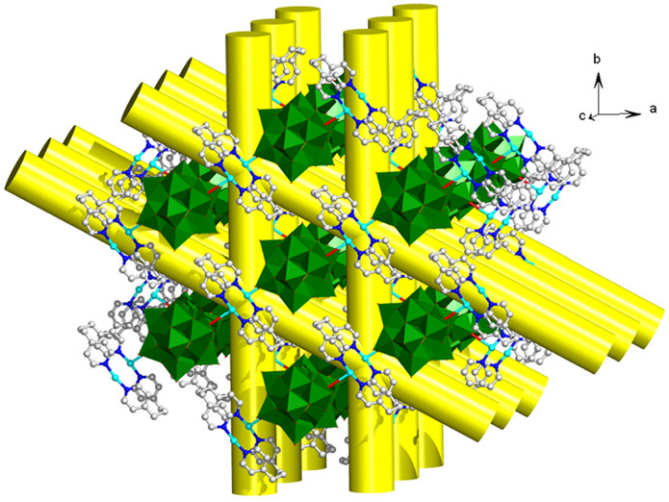

Fig. 5. View the 3D framework structure of **1**.

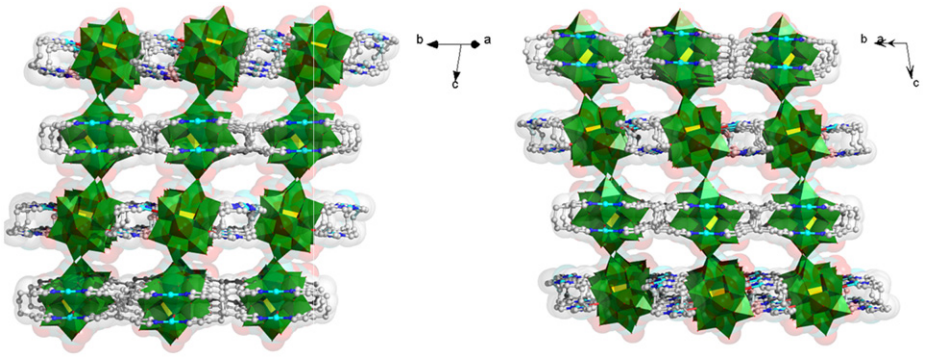

Fig. 4. The space-filling models showing the unusual framework with two-directional channels.

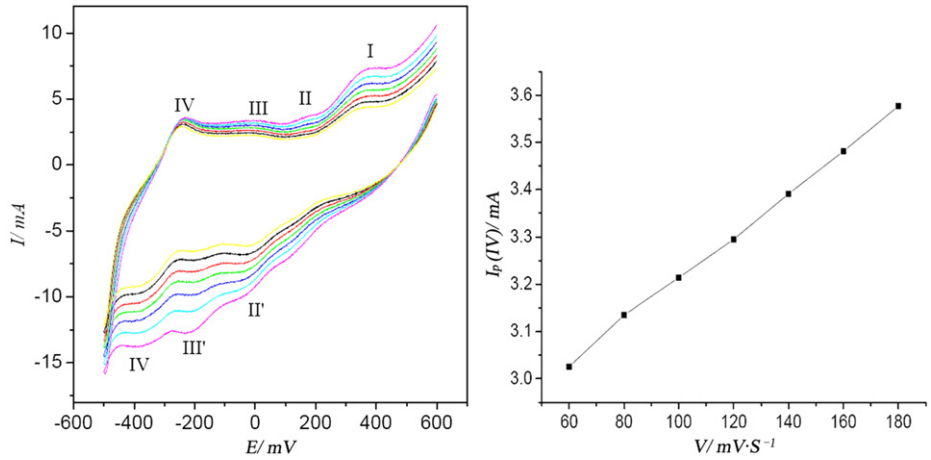

Fig. 6. (Left) Cyclic voltammograms of the **1**-CPE in the 1 M H_2SO_4 solution at different scan rates (from inner to outer: 60, 80, 100, 120, 140, 160, and 180 mV s^{-1}) and (right) the dependence of anodic peak IV current on scan rates.

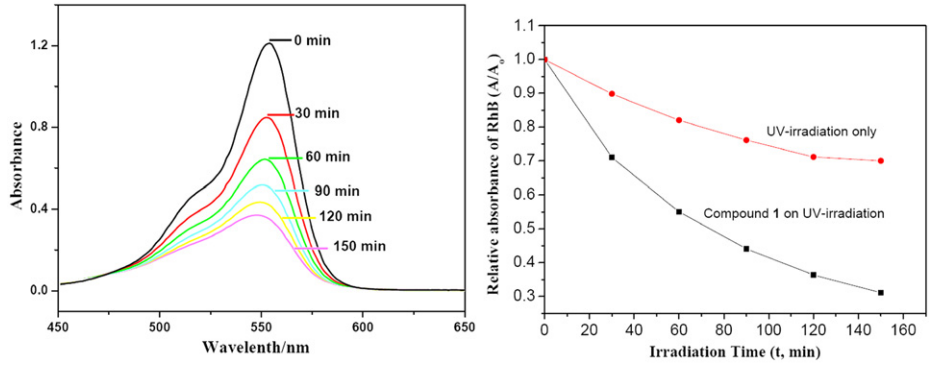

Fig. 7. (Left) The UV–visible absorption spectral changes for the RhB solutions as a function of irradiation time in the presence of **1**. (Right) The plot of relative absorbance (A/A_0) of the RhB solution on UV-irradiation *versus* reaction time in the presence of **1** and absence of **1**.

wastewater. The photocatalytic performance of **1** against photodegradation of RhB under UV irradiation has been checked through a typical process: prior to photocatalytic experiment, 150 mg of **1** was mixed together with 90 ml of 10.0 mg/L RhB solution in a beaker by ultrasonic dispersion for 0.5 h. The mixture was stirred for 2 h till reached the surface-adsorption equilibrium on the particles of **1**. Then, the mixture was stirred continuously under ultraviolet (UV) irradiation from a 125 W high pressure Hg lamp at a distance of 4–5 cm between the liquid surface and the lamp. Every 30 min, 3.0 ml of the sample was taken out from the beaker, followed by several centrifugations to remove compound **1**, and a clear solution was obtained for analysis. As shown in Fig. 7 left, the absorption peak of RhB decreased obviously from 1.21 to 0.37. Moreover, the relative absorbance of RhB (A/A_0) *versus* reaction time (t) was plotted (Fig. 7 right). The conversion of RhB (η) can be expressed by the following equation [64]: $\eta=[(A_0-A)/A_0]\times 100\%$, where A_0 is the initial absorbency of the RhB solution corresponding to the maximum absorption wavelength; A is the absorbency of RhB solution after UV light irradiation at any time. The calculation results show that ca. 68.5% of RhB had been decomposed after irradiation for 2.5 h. It reveals that compound **1** is outstanding photocatalyst for photocatalytic degradation of RhB. The possible mechanism of photodegradation of RhB by **1** as catalyst are as follows: Compound **1** is constructed by mono-substituted Keggin ployoxometalate anions ($PW_{11}Cu$ chains) and 24-membered $(Cubpp)_2$ cation-macrocycles. So like other polyoxometalates, $PW_{11}Cu$ in **1** possesses very similar photochemical characteristics of the semiconductor photocatalysts, having large gaps (ca. 4.94 eV, estimated by the UV spectrum of **1**, see Fig. S7), d^0 transition metal atoms, and oxygen atoms. When **1** is photoactivated by irradiation of its surface with the light energy higher than or equal to its band gap energy, the charge transfer from an O^{2-} ion to a W^{6+} ion will occur at W–O–W bonds, and engender excited-state $PW_{11}Cu$ with a pair of hole center (O^-) and trapped electron center (W^{5+}). The excited-state $PW_{11}Cu$ (e^-+h^+) is a more powerful oxidant to be able to degrade RhB [61,65–68].

In addition, the photodegradation process of RhB in the absence of the compound **1** with UV-irradiation only have also been done as shown in Fig. S8. The RhB molecules were degraded with UV-irradiation only, but these degradation rate is low when compared to the same conditions except for presence of **1** (Fig. 7 right). The results indicate that compound **1** is a good photocatalyst for degradation of RhB. Recently, a kind of semiconductor inorganic material in nanometric scale (usually oxides modified TiO_2 nanoparticles) is used as catalyst to promote the degradation/oxidation of the organic dyes [69]. For example, a well work reported by Libanori et al. in which the commercial TiO_2 nanoparticles were superficially modified through polymeric resins obtained from polymerization of citrate complexes of Y^{3+} and Al^{3+} with ethyleneglycol and such surface modifier played an important role in the photodegradation kinetic process of RhB [70]. In comparison with the example mentioned above, compound **1** shows slightly lower photocatalytic activities than unmodified TiO_2 nanoparticles and optimum Y_2O_3 and Al_2O_3 modified TiO_2 nanoparticles, but compound **1** exhibits much higher photocatalytic activities than the single Y_2O_3 and Al_2O_3 and possesses comparable photocatalytic activities with the most

of Y_2O_3 or Al_2O_3 modified TiO_2 nanoparticles. Furthermore, compared with theses oxides (Y_2O_3 and Al_2O_3, and their modified TiO_2 nanoparticles), compound **1** as a catalyst to degrade organic dyes may be a low toxicity and its behavior as a kind of environmentally benign catalyst.

4. Conclusions

In summary, a new mono-substituted Keggin anion-chain based inorganic–organic hybrid compound has been obtained. Notably, it exhibits two structural features. First, the neighboring mono-substituted Keggin clusters are alternately connected via sharing the oxygen atoms to form a –A–B–A–B– array chain, which is different from the former –A–A–A–A– array ones; second, the mono-substituted Keggin anion-chains are linked by the 24-membered $(Cubpp)_2$ macrocycles to form a 3D framework. The preparation of **1** offers a feasible route for synthesis of high dimensional mono-substituted Keggin anion-chain based inorganic–organic hybrid compounds. A further work in this field is underway.

Acknowledgments

This work was financially supported by the National Science Foundation of China (nos. 21071038 and 21101045), Science and Technology Innovation Foundation of Harbin (no. 2010RFLXG004), the Foundation of Education Committee of Heilongjiang (no. 11531228), and Heilongjiang Postdoctoral Science Foundation (no. LBH-Q09069).

Appendix A. Supporting materials

Supplementary data associated with this article can be found in the online version at doi:10.1016/j.jssc.2011.11.032.

References

[1] M.T. Pope, Heteropoly, Isopoly Oxometalates, Springer Verlag, New York, 1983.
[2] M.T. Pope, A. Müller (Eds.), Polyoxometalate Chemistry from Topology via Self-Assembly to Applications, Kluwer Academic Publishers, Dordrecht, 2001.
[3] M.T. Pope, A. Müller, Polyoxometalate Chemistry: from Topology via Self-Assembly to Applications, Kluwer, Dordrecht, The Netherlands, 2001.
[4] E. Coronado, C.J. Gómez-García, Chem. Rev. 98 (1998) 273.
[5] A. Müller, P. Kögerler, Coord. Chem. Rev. 199 (2000) 335.
[6] D.L. Long, E. Burkholder, L. Cronin, Chem. Soc. Rev. 36 (2007) 105.
[7] D.L. Long, R. Tsunashima, L. Cronin, Angew. Chem. Int. Ed. 49 (2010) 1736.
[8] V. Artero, A. Proust, P. Herson, F. Villain, C. Moulin, P. Gouzerh, J. Am. Chem. Soc. 125 (2003) 11156.
[9] C. Besson, Z.Q. Huang, Y.V. Geletii, S. Lense, K.I. Hardcastle, D.G. Musaev, T.Q. Lian, A. Proustac, C.L. Hill, Chem. Commun. 46 (2010) 2784.
[10] K. Kamata, Y. Nakagawa, K. Yamaguchi, N. Mizuno, J. Am. Chem. Soc. 130 (2008) 15304.
[11] D.B. Dang, Y. Bai, C. He, J. Wang, C.Y. Duan, J.Y. Niu, Inorg. Chem. 49 (2010) 1280.
[12] Y.H. Guo, C.W. Hu, J. Mol. Catal. A 262 (2007) 136.
[13] C.Y. Sun, S.X. Liu, D.D. Liang, K.Z. Shao, Y.H. Ren, Z.M. Su, J. Am. Chem. Soc. 131 (2009) 1883.
[14] R.D. Gall, C.L. Hill, J.E. Walker, Chem. Mater. 8 (1996) 2523.
[15] Special issue on polyoxometalates, C.L. Hill (guest editor), Chem. Rev. 98 (1998) 1.
[16] E.D. Clercq, Rev. Med. Virol. 10 (2000) 255.
[17] J.T. Rhule, C.L. Hill, D.A. Judd, Chem. Rev. 98 (1998) 327.
[18] X. Wang, J. Liu, M. Pope, Dalton Trans. (2003) 957.
[19] A. Proust, R. Thouvenot, P. Gouzerh, Chem. Commun. (2008) 1837.
[20] J. Zhang, Y.F. Song, L. Cronin, T.B. Liu, J. Am. Chem. Soc. 130 (2008) 14408.
[21] J. Zhang, J. Hao, Y.G. Wei, F.P. Xiao, P.H. Yin, L.S. Wang, J. Am. Chem. Soc. 132 (2010) 14.
[22] P. Mialane, A. Dolbecq, F. Sécheresse, Chem. Commun. (2006) 3477.
[23] B.S. Bassil, S.S. Mal, M.H. Dickman, U. Kortz, H. Oelrich, L. Walder, J. Am. Chem. Soc. 130 (2008) 6696.
[24] X. Fang, P. Kögerler, L. Isaacs, S. Uchida, N. Mizuno, J. Am. Chem. Soc. 131 (2009) 432.
[25] J.W. Zhao, H.P. Jia, J. Zhang, S.T. Zheng, G.Y. Yang, Chem. Eur. J. 13 (2007) 10030.
[26] Y.Y. Bao, L.H. Bi, L.X. Wu, J. Solid State Chem. (2011). doi:10.1016/j.jssc.2011.01.011.
[27] A. Dolbecq, E. Dumas, C.R. Mayer, P. Mialane, Chem. Rev. 110 (2010) 6009 and references therein.
[28] R.M. Yu, X.F. Kuang, X.Y. Wu, C.Z. Lu, J.P. Donahue, Coord. Chem. Rev. 253 (2009) 2872 and references therein.
[29] H.Y. An, E.B. Wang, D.R. Xiao, Angew. Chem. Int. Ed. 45 (2006) 904.
[30] J.Y. Niu, M.L. Wei, J.P. Wang, Eur. J. Inorg. Chem. (2004) 160.
[31] X.L. Wang, C. Qin, E.B. Wang, Z.M. Su, Chem. Commun. (2007) 4245.
[32] I.S. Lee, J.R. Long, S.B. Prusiner, J.G. Safar, J. Am. Chem. Soc. 127 (2005) 13802.
[33] H.J. Pang, J. Peng, C.J. Zhang, Y.G. Li, P.P. Zhang, H.Y. Ma, Z.M. Su, Chem. Commun. 46 (2010) 5097.
[34] C.M. Liu, D.Q. Zhang, D.B. Zhu, Cryst. Growth Des. 5 (2005) 1639.
[35] Q.G. Zhai, X.Y. Wu, S.M. Chen, Z.G. Zhao, C.Z. Lu, Inorg. Chem. 46 (2007) 5046.
[36] D. Hagrman, P.J. Hagrman, J. Zubieta, Angew. Chem. Int. Ed. 38 (1999) 3165.
[37] C.Y. Duan, M.L. Wei, D. Guo, C. He, Q.J. Meng, J. Am. Chem. Soc. 132 (2010) 3321.
[38] C.H. Li, K.L. Huang, Y.N. Chi, X. Liu, Z.G. Han, L. Shen, C.W. Hu, Inorg. Chem. 48 (2009) 2010.
[39] G. Férey, C. Mellot-Draznieks, C. Serre, F. Millange, J. Dutour, S. Surblé, I. Margiolaki, Science 309 (2005) 2040.
[40] L.S. Long, CrystEngComm 12 (2010) 1354.
[41] C. Pichon, A. Dolbecq, P. Mialane, J. Marrot, E. Rivière, M. Goral, M. Zynek, T. McCormac, S.A. Borshch, E. Zueva, F. Sécheresse, Chem. Eur. J. 14 (2008) 3189.
[42] D. Laurencin, R. Villanneau, H. Gérard, A. Proust, J. Phys. Chem. A 110 (2006) 6345.
[43] Z.G. Han, Y.L. Zhao, J. Peng, H.Y. Ma, Q. Liu, E.B. Wang, N.H. Hu, H.Q. Jia, Eur. J. Inorg. Chem. (2005) 264.
[44] Z.G. Han, Y.L. Zhao, J. Peng, H.Y. Ma, Q. Liu, E.B. Wang, J. Mol. Struct. 738 (2005) 1.
[45] J. Peng, H.Y. Ma, Z.G. Han, B.X. Dong, W.Z. Li, J. Lu, E.B. Wang, Dalton Trans. (2003) 3850.
[46] S. Reinoso, P. Vitoria, L.S. Felices, L. Lezama, J.M. Gutiérrez-Zorrilla, Chem. Eur. J. 11 (2005) 1538.
[47] B.B. Yan, Y. Xu, X.H. Bu, N.K. Goh, L.S. Chia, G.D. Stucky, J. Chem. Soc. Dalton Trans. (2001) 2009.
[48] Y. Lu, Y. Xu, E.B. Wang, J. Lü, C.W. Hu, L. Xu, Cryst. Growth Des. 5 (2005) 257.
[49] L.S. Felices, P. Vitoria, J.M. Gutiérrez-Zorrilla, L. Lezama, S. Reinoso, Inorg. Chem. 45 (2006) 7748.
[50] G.M. Sheldrick, SHELXL-97, Program for Crystal Structure Refinement, University of Göttingen, Germany, 1997.
[51] G.M. Sheldrick, SHELXS-97, Program for Solution of Crystal Structures, University of Göttingen, Germany, 1997.
[52] I.D. Brown, D. Altermatt, Acta Crystallogr. B (1985) 4124.
[53] C.D. Wu, C.Z. Lu, H.H. Zhuang, J.S. Huang, Inorg. Chem. 41 (2002) 5636.
[54] C.J. Zhang, H.J. Pang, Q. Tang, H.Y. Wang, Y.G. Chen, New J. Chem. 35 (2011) 190.
[55] J.Q. Sha, J. Peng, Y.Q. Lan, Z.M. Su, H.J. Pang, A.X. Tian, P.P. Zhang, M. Zhu, Inorg. Chem. 47 (2008) 5145.
[56] (a) Y.V. Zefirov, Russ. J. Inorg. Chem. 45 (2000) 1552;
(b) S.Z. Hu, C.H. Zhou, Q.R. Cai, Acta Phys. Sin. 19 (2003) 1073.
[57] H.J. Pang, C.J. Zhang, J. Peng, Y.H. Wang, J.Q. Sha, A.X. Tian, P.P. Zhang, Y. Chen, M. Zhu, Z.M. Su, Eur. J. Inorg. Chem. (2009) 5175.
[58] C. Rocchiccioli-Deltcheff, M. Fournier, R. Franck, R. Thouvenot, Inorg. Chem. 22 (1983) 207.
[59] R. Massart, R. Contant, J.M. Fruchart, J.P. Ciabrini, M. Fournier, Inorg. Chem. 16 (1977) 2916.
[60] M.T. Pope, G.M. Varga, Inorg. Chem. 5 (1966) 1249.
[61] T. Rüther, V.M. Hultgren, B.P. Timko, A.M. Bond, W.R. Jackson, A.G. Wedd, J. Am. Chem. Soc. 125 (2003) 10133.
[62] A.X. Tian, J. Ying, J. Peng, J.Q. Sha, Z.G. Han, J.F. Ma, Z.M. Su, N.H. Hu, H.Q. Jia, Inorg. Chem. 47 (2008) 3274.
[63] Z.G. Han, Y.L. Zhao, J. Peng, Y.H. Feng, J.N. Yin, Q. Liu, Electroanalysis 17 (2005) 1097.
[64] R.M. Mohamed, A.A. Ismail, I. Othman, I.A. Ibrahim, J. Mol. Catal. A Chem. 238 (2005) 151.
[65] Y.H. Guo, Y.H. Wang, C.W. Hu, Y.H. Wang, E.B. Wang, Y.C. Zhou, S.H. Feng, Chem. Mater. 12 (2000) 3501.
[66] W.J. Li, D.Z. Li, S.G. Meng, W. Chen, X.Z. Fu, Y. Shao, Environ. Sci. Technol. 45 (2011) 2987.
[67] R.R. Ozer, J.L. Ferry, Environ. Sci. Technol. 35 (2001) 3242.
[68] T. Yamase, Chem. Rev. 98 (1998) 307.
[69] A.F. Nogueira, C. Longo, M.-A.D. Paoli, Coord. Chem. Rev. 248 (2004) 1455.
[70] R. Libanori, T.R. Giraldi, E. Longo, E.R. Leite, C. Ribeiro, J. Sol–Gel Sci. Technol. 49 (2009) 95.